Single electrode entropy change for $LiCoO_2$ electrodes

Frank Richter[a], Astrid Fagertun Gunnarshaug[a], Odne S. Burheim[b], Preben J. S. Vie[c] and Signe Kjelstrup[*a]

[a]PoreLab, Department of Chemistry, Norwegian University of Science and Technology, NTNU, Trondheim, Norway

[b]Department of Energy and Process Technology, Norwegian University of Science and Technology, NTNU, Trondheim, Norway
[c]IFE, Institute for Energy Technology, Kjeller, Norway

Heat effects are known to be crucial for the performance of the Li-battery. In addition to the irreversible effects (*e.g.* Joule heat), reversible heat effects may play a role. These effects, i.e. the Soret and Seebeck effects, are however scarcely investigated. We report the initial and stationary state thermoelectric potentials of a pouch cell having electrodes where Li is intercalated in CoO_2. The electrolyte consists of 1.0 M lithium hexafluoro phosphate dissolved in a mixture of equal volumes of ethylene carbonate and diethyl carbonate. The two identical electrodes were thermostatted at different temperatures, the average being always 298 K and the potential was measured over several days. We observe two time-dependent phenomena with characteristic times of 4.5 and 21.3 hours. We explain them by thermal diffusion of salt and esters. The Seebeck coefficient varies from -2.8 mV/K in the initial state to 1.5 mV/K in the state characterized by partial Soret equilibrium. The time-variation of the signal is used to compute Seebeck coefficients, the contributions to the heats of transfer, and the reversible heat effect at the $LiCoO_2$-and carbon electrodes. The electrode heat effects in a Li-battery is surprisingly asymmetric, given the small entropy of the total reaction. The $LiCoO_2$ electrode heat varies from 51 to - 46 kJ/mol, while the carbon electrode will vary from -73 to 56 kJ/mol. Uncertainties in computations are within 15%. This may explain why the reaction entropy depends largely on the state of charge. It may also be important for thermal modeling of the battery.

[*]Corresp. Author, e-mail: signe.kjelstrup@ntnu.no

Introduction

The use of lithium rechargeable batteries in electric vehicles, hybrid electric vehicles or hybrid electric ships puts thermal management issues into focus. The faster the battery cycle is repeated, and the larger the battery packs are, the more important the thermal management issues become. Thermal modeling is thus intensely discussed in the literature, in the context of *e.g.* cell design, material use, and type of application (1–8).

At high current densities, the most important thermal effects are due to ohmic resistances (Joule heat), or resistances to the electrode reactions (as reflected in the overpotential), These effect are always positive, as they are connected with dissipation of energy. The change in entropy of the battery reaction; i.e. the reaction entropy, is a reversible heat source or heat sink (9) which depends on the state of charge (SOC) of the battery. The average entropy of reaction for a charging cycle in the Li battery with Li_xCoO_2 and carbon electrodes is 36 J/K mol (9), corresponding to a heat effect of 10.7 kJ/mol at 298 K. The value changes sign as the reaction is reversed, from charging to discharging operations. This may even lead to local cooling (10). The origin of this is the Peltier effect, but also Soret effects may play a role (11). The Peltier and Soret heat effects are difficult to measure directly (12, 13), but can be achieved through their relation to the Seebeck coefficient of the cell (11, 14, 15). This requires that the cell processes are described in terms of irreversible thermodynamics. The Seebeck coefficient can then be measured with good accuracy.

There are only a few reports in the literature on the single electrode Peltier heats in Li-battery related cells (12, 16), even if the topic of single electrode heats was much studied in the past, see (17) and references therein. Motohashi and co-workers (16) measured the Seebeck coefficient, using Li_xCoO_2 as an electrolyte at 293 K. Here x is the molar ratio of Li to CoO_2. The Seebeck coefficient varied with x between 70-100 $\mu V/K$ when $0.94 \leq x \leq 0.98$. A rapid decrease from 90 to 10 $\mu V/K$ took place when x was changed from 0.75 to 0.50. The results were obtained using a "steady-state technique" which was not explained in more detail.

Huang *et al.* measured the calorimetric heat effect in various battery cells with electrodes of Li_yC_6 and Li_xCoO_2. They also determined the thermoelectric potential of a cell with Li_xCoO_2 electrodes and an electrolyte of 1 M lithium hexafluorophosphate ($LiPF_6$) in a mixture of equal volumes of ethylene carbonate and diethyl carbonate (EC, DEC (v/v = 1:1)). Their positive Seebeck coefficient, 1.17 mV/K, corresponds to a Peltier heat at 298 K equal to -33.66 kJ/mol. They did not report how long the measurements lasted.

In this paper, we report the Seebeck coefficient of the same symmetrical cell as used by Huang et al. The cell has $LiCoO_2$- electrodes (x = 1) and the electrolyte is the same. The cells have not been investigated earlier over time (days). In a ternary mixture of a salt and two organic compounds, there is bound to be diffusion, including also thermal diffusion. The presence of a temperature gradient; a thermal driving force, might then lead to separation of components. Self diffusion coefficients reported in the literature vary in order of magnitude from 10^{-10} to 10^{-9} m^2s^{-1} (18). Diffusion will affect the thermoelectric signal, as prescribed by irreversible thermodynamics theory.

Knowledge of these effects is essential for development of precise battery models. The experimental determination of properties to be used in such models, is the main motivation for this work. A secondary motivation, more farfetched, is to contribute to the study of thermoelectric cells with ionic liquids. Thermoelectric cells can, as one of the few devices, convert low-temperature industrial waste heat into electric power. Commercially available thermoelectric generators are currently mostly of a semiconductor type, with Seebeck coefficients that typically are some μV/K (19). Research on ion-conducting materials for thermoelectric power generator purposes, which give larger Seebeck-coefficients, is therefore of general interest.

The work is outlined as follows. In order to decompose the experimental data, we need the basic equations provided in irreversible thermodynamics. These are therefore presented first. The detailed presentation of the experimental cell and measurement conditions follow, before the data are decomposed and discussed. We shall see that the Seebeck coefficients are large, and that there are large contributions from the heats of transfer that even may change the sign of the coefficient.

The thermoelectric cell

The cell of interest has two identical electrodes, consisting of Li(s) intercalated in CoO_2(s). There is one mol Li per mole CoO_2. The electrolyte contains 1M $LiPF_6$ dissolved in a solvent consisting of 50 : 50 volume % of ethylene carbonate (EC) and diethyl carbonate (DEC). In a mixture of 1 M $LiClO_4$ (20), a Li^+-ion is surrounded by on the average 3 EC and one DEC molecule. The esters have a dipole moment, but do not dissociate into ions. We assume they do not contribute to charge transfer directly, but they may be transported electrophoretically along with the ion(s). The electrolyte is held in place in a filter consisting of glass microfibers. The electrodes are connected to the outer circuit via thermostatted aluminum plates. The thermostatting takes place via copper end plates. The potentiometer has the temperature of the environment, T_0, see Fig.1.

The phases in the cell are denoted as follows: Symbol (a) is used for the anode, (s) for the surface or interface, (e) for the electrolyte, and (c) for the cathode. The left-hand side aluminum current lead has temperature T and the right-hand side aluminum connecting lead has temperature $T+\Delta T$, where $\Delta T = T^{c,e} - T^{a,e}$, see Fig. 1. Superscript pairs refers first to the phase in question and after comma to the neighboring phase. Superscript e,c means therefore a variable in the e-phase taken close to the phase c. As the electrode surface is taken the region containing $LiCoO_2$.

The cell is with standard notation

$$\mathrm{Al(s},T) \mid \mathrm{LiCoO_2(s},T) \mid \mathrm{EC,DEC,LiPF_6} \mid \mathrm{LiCoO_2(s},T+\Delta T) \mid \mathrm{Al(s},T+\Delta T) \qquad [1]$$

The identical electrodes and the connecting leads are thermostatted at temperature T and $T+\Delta T$, respectively. Within one electrode (surface), there is ideally no temperature gradient, cf. Section 3. The difference in temperature is ideally across the electrolyte.

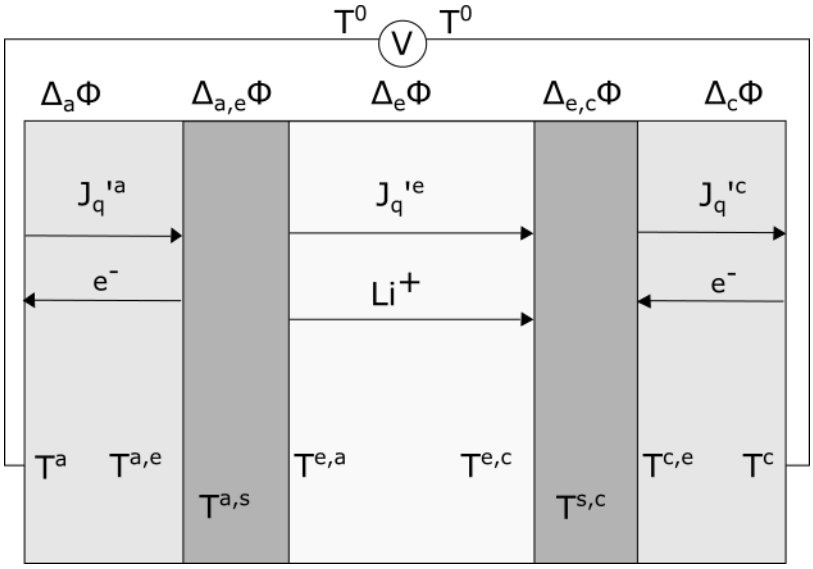

Figure 1. The electrochemical system schematically. The two end pieces consists of aluminum (Al), the electrode layer of $LiCoO_2$, and the electrolyte layer of 1M $LiPF_6$ dissolved in a solvent consisting of 50 : 50 volume % of ethylene carbonate (EC) and diethyl carbonate (DEC). The electrolyte is held in place by a microporous layer consisting of glass microfibers. The notation, used to locate transport properties to the phases, are a (anode), c (cathode), s (surface) and e (electrolyte). Superscript pairs refer first to the phase in question and next to the neighboring phase. Superscript e,c means therefore a variable in the e-phase taken close to the phase c.

The electrode reaction on the left-hand side produces eventually one mole of electrons in the Al(s) and one mole of ions in the electrolyte:

$$\mathrm{Li(CoO_2)} \rightleftharpoons \mathrm{Li^+(PF_6^-)} + \mathrm{e^-(Al)} \qquad [2]$$

The reaction takes place somewhere in the region bounded by Al and the electrolyte, the region that we name the electrode surface.

The Seebeck coefficient is obtained from a potential measurement at negligible current density. The cell changes under these conditions are therefore reversible. The potential measurement is, as we shall see, well defined under initial time and infinite time steady state conditions. The electrode reaction rate is $r^s = j/F$.

At initial times, the electrolyte is homogeneous, and there are no gradients in chemical potentials. At infinite time, a gradient in the electrolyte, $LiPF_6$, even in EC and DEC, may have risen as a consequence of the temperature gradient that is applied to the system. At a certain time, the transport of components will stop. The thermal driving force is then counterbalanced by a gradient in solute (and solvent) chemical potential. To move charge against this gradient may also contribute to the Seebeck coefficient, as we shall see. The electrolyte conducts charge by Li^+ and PF_6^{-1}.

The Seebeck coefficient

The measured cell potential has five contributions, two from the connecting leads (of Cu-Al), two from the electrode interfaces, and one from the electrolyte. The contributions are additive and independent of the frame of reference chosen, and we write:

$$\Delta\phi = \Delta_{\mathrm{l}}\phi + \Delta_{\mathrm{a,e}}\phi + \Delta_{\mathrm{e}}\phi + \Delta_{\mathrm{e,c}}\phi + \Delta_{\mathrm{r}}\phi \qquad [3]$$

Subscripts used with Δ refer to the locations at which the difference is taken. Subscripts i,k means the value in phase k minus the value in phase i. The Seebeck coefficient is defined as

$$\varepsilon = \left(\frac{\Delta\phi}{\Delta T}\right)_{j=0} \qquad [4]$$

where $\Delta T = T^{s,c} - T^{s,a}$. In the following we shall give expressions for all contributions to $\Delta\phi$, see (21, 22) for more details.

Basic equations

The symmetrical electrochemical cell is exposed to a temperature gradient by thermostatting the electrodes to different temperatures. After a transient period lasting some 10 minutes, a temperature gradient is established across the materials (see the experimental section below). In the most complex part of the system, the electrolyte, there is transport of heat, charge as well as mass. The electrolyte as a ternary mixture containing $LiPF_6$ and two organic carbonates, EC and DEC inside a microporous glass filter. The third component is chosen as the frame of reference for the transport. For the time being we do not assign the other two to any number. The three chemical potentials are related by the Gibbs-Duhem equation.

The entropy production σ of the electrolyte (e) is then:

$$\sigma = J_q'\left(\frac{\partial}{\partial x}\frac{1}{T}\right) + J_1\left(-\frac{1}{T}\frac{\partial\mu_{1,T}}{\partial x}\right) + J_2\left(-\frac{1}{T}\frac{\partial\mu_{2,T}}{\partial x}\right) + j\left(-\frac{1}{T}\frac{\partial\phi}{\partial x}\right) \qquad [5]$$

The chemical potential of a salt j is

$$\mu_j = \mu_j^0 + RT\ln c_j^2\gamma_{\pm,j}^2 \qquad [6]$$

where μ_j^0 is the standard chemical potential. The activity of the component is that of an ideal electrolyte times the activity coefficient, $a_j = c_j^2\gamma_{\pm,j}^2$, where c_j is the concentration of the ions and $\gamma_{\pm,j}$ is the mean ionic activity coefficient. The chemical potential of EC or DEC is

$$\mu_i = \mu_i^0 + RT\ln c_i\gamma_i \qquad [7]$$

It follows from standard non-equilibrium thermodynamics that the measurable heat flux $J_q'^i$, the mass fluxes of 1 and 2, and the electric potential gradient are linear combina-

tions of the conjugate driving forces. We write:

$$J_q' = l_{qq}\left(-\frac{1}{T^2}\frac{\partial T}{\partial x}\right) + l_{q1}\left(-\frac{1}{T}\frac{\partial \mu_{1,T}}{\partial x}\right) + l_{q2}\left(-\frac{1}{T}\frac{\partial \mu_{2,T}}{\partial x}\right) + \pi(j/F) \quad [8]$$

$$J_1 = l_{1q}\left(-\frac{1}{T^2}\frac{\partial T}{\partial x}\right) + l_{11}\left(-\frac{1}{T}\frac{\partial \mu_{1,T}}{\partial x}\right) + t_1(j/F) \quad [9]$$

$$J_2 = l_{2q}\left(-\frac{1}{T^2}\frac{\partial T}{\partial x}\right) + l_{22}\left(-\frac{1}{T}\frac{\partial \mu_{2,T}}{\partial x}\right) + t_2(j/F) \quad [10]$$

$$\frac{\partial \phi}{\partial x} = -\frac{\pi}{FT}\frac{\partial T}{\partial x} - \frac{t_1}{F}\frac{\partial \mu_{1,T}}{\partial x} - \frac{t_2}{F}\frac{\partial \mu_{2,T}}{\partial x} + rj \quad [11]$$

The Onsager relation applies ($l_{ij} = l_{ji}$). We neglect for simplicity the impact of component 1 on the diffusion of component 2, setting $l_{12} = l_{21} = 0$.

The electric potential gradient (the last equation) has contributions from the Peltier heat, π, and the gradients in the chemical potential of $LiPF_6$ and EC. These terms contribute once the mixture is no longer homogeneous. This happens when the components start their diffusion in the thermal field.

The coefficients are found from experiments. The ohmic resistivity r is not relevant in an *emf*-experiment. The thermal conductivity of a uniform material is denoted by k, the Peltier coefficient is π, and the transference coefficient of the components are t_1, t_2:

$$r = -\left(\frac{\partial \phi/\partial x}{j}\right)_{dT=0} \quad [12]$$

$$\pi = \left(\frac{J_q'}{j/F}\right)_{dT=0} \quad [13]$$

$$k = -\left(\frac{J_q'}{\partial T/\partial x}\right)_{j=0} \quad [14]$$

$$t_i = \left(\frac{J_i}{j/F}\right)_{dT=0, d\mu_{i,T}=0} \quad i = 1,2 \quad [15]$$

The transference coefficient of component i is the number of moles of i that is transported per one mole of electrons that is passing in the external circuit. For the salt transference coefficient t_i can be interpreted by the Li^+-ion transport number (23). The electrode reaction consumes 1 mol of Li^+ per one mole of e^- produced on the right-hand side. The reaction is reversed at the left-hand side. With the surface frame of reference $t_i = 1 - t_{Li^+}$. The EC and DEC-molecules may be carried along electrophoretically with the ions. The sign of t_i gives information about the direction that the component is moved. A negative value means that the component moves opposite of the positive charge carrier, like is the case here for LiCl, when the electrodes are reversible to the Li^+-ion.

In the absence of an electric current and at isothermal conditions, we define the heat of transfer for the components

$$q_i^* = \left(\frac{J_q'}{J_i}\right)_{j=0, dT=0} \quad i = 1,2 \quad [16]$$

The heat of transfer of component i, q_i^*, in kJ/mol, is connected with the thermal diffusion and interdiffusion of i in the separator matrix

$$q_i^* = RT^2 D_{T,i}/D_i \;\; i = 1,2 \qquad [17]$$

Soret equilibrium for the two components is defined for $J_1 = J_2 = 0, j = 0$. Here D_i is the diffusion coefficient in the chosen frame of reference, while $D_{T,i}$ is the thermal diffusion coefficient. We obtain from Eqs. (8 and 9)

$$\left(\frac{d\mu_{i,T}}{dx}\right)_{J_i=0, j=0} = -\frac{q_i^*}{T}\frac{dT}{dx} \quad i = 1,2 \qquad [18]$$

These chemical potential gradients in the electrolyte at $j \approx 0$ enter the expression for the Seebeck coefficient together with the Peltier heat in Eq.(10).

Electronic connector contributions

In the electronic conductors, there is coupled transport of heat and charge. In the electronic conductors there is no mass transport, and there are only two fluxes (of heat and charge) and their conjugate driving forces. The reversible heat effect can then be interpreted as the entropy transported by the electrons in the conductor;

$$\pi^l = -TS_e^* \qquad [19]$$

The negative sign is chosen so that the transported entropy of the electron, S_e^*, is positive. It signifies the heat transported along with the electron. There is no gradient in composition in the conductor, so this is the sole contribution to the Seebeck coefficient. The potentiometer temperature is T^0. The contribution on the left-hand side conductor becomes $\Delta_l\phi = -S_e^*(T - T^0)$. The corresponding contribution on the right-hand side is $\Delta_r\phi = -S_e^*(T^0 - T - \Delta T)$. The combined contribution is accordingly

$$\Delta_l\phi + \Delta_r\phi = S_e^*\Delta T \qquad [20]$$

Li_xCoO_2 is a semiconductor when $x > 0.94$ as here (12). The Seebeck-coefficient of the semi-conductor connected to aluminum-connecting leads was measured at 300 K to 100 μV/K (12). We shall therefore use $S_e^* = 10$ J/K mol.

Electrolyte contributions

In the start of the experiment, the electrolyte and solvent concentrations are ideally speaking uniform. There has been no time for diffusion and establishment of a chemical potential gradient. This does then not contribute to the electric potential drop and we have:

$$\varepsilon_0^{\mathrm{el}} = \left(\frac{\Delta_e\phi}{\Delta T}\right)_{j=0, d\mu_{1,T}=0, d\mu_{1,T}=0} = -\frac{\pi}{TF} \qquad [21]$$

Two time-dependent phenomena can be observed (cf. the results section), and they can be separated on the time-scale. One gradient in chemical potential is then established before the other. We assume that the gradient in component 1 is first established. The EC and DEC have higher self diffusion coefficients than the ions (18), so EC is a potential candidate for component 1. At stationary state after some time, $J_1 = 0$. Only the gradient in chemical potential of 1 contributes then to the *emf*. The contribution can be expressed by the temperature gradient, using Eq.18 with (8)

$$\varepsilon^{\mathrm{el}}_{\infty,1} = \left(\frac{\Delta_e \phi}{\Delta T}\right)_{j=0,J_1=0} = -\frac{\pi - t_1 q_1^*}{TF}\Delta T \qquad [22]$$

The second slower time-dependent phenomenon will eventually add a term to this expression, giving:

$$\varepsilon^{\mathrm{el}}_{\infty,2} = \left(\frac{\Delta_e \phi}{\Delta T}\right)_{j=0,J_1=J_2=0} = -\frac{\pi - t_1 q_1^* - t_2 q_2^*}{TF} \qquad [23]$$

At stationary state, infinite time (when all time-dependent phenomena have relaxed), there is a simpler interpretation of the net reversible heat transfer connected with the electrodes. We can find this expression, realizing that the value of the *emf* is independent of the choice of frame of reference for the transports. Assume therefore as an alternative that all anions are fixed in a position. Only Li^+ is then jumping via one anion to another through a quasi-anion lattice. Therefore, only Li^+ contributes to the reversible heat transport. The Li^+ moves in the direction of the positive current. This gives

$$\varepsilon^{\mathrm{el}}_{\infty,2} = \left(\frac{\Delta_e \phi}{\Delta T}\right)_{j=0,J_1=0,J_2=0} = -\frac{S^*_{\mathrm{Li}^+}}{F} \qquad [24]$$

where $S^*_{\mathrm{Li}^+}$ is the transported entropy of Li^+. The transported entropy is likely to be a function of the electrolyte composition. This allows the identification:

$$(\pi - t_1 q_1^* - t_2 q_2^*)_{j=0,J_1=J_2=0} = T S^*_{\mathrm{Li}^+} \qquad [25]$$

From this relation it follows that;

$$\pi^e = T S^*_{\mathrm{Li}^+} + t_1 q_1^* + t_2 q_2^* \qquad [26]$$

From this we can write the contribution to the Seebeck coefficient at initial time

$$\varepsilon^{\mathrm{el}}_0 = -(S^*_{\mathrm{Li}^+} + (t_1 q_1^* + t_2 q_2^*)/T)\Delta T \qquad [27]$$

The terms in this equation determine the thermoelectric potential.

Electrode surface contributions

In the thermodynamic description of the electrode surface, we consider Li(s) intercalated in CoO_2 as an infinitely thin phase between the electrolyte and the electronic conductor, which consists of a plate of aluminum. The excess entropy production of the electrode surfaces

refers to Li(s) intercalated in CoO_2 in contact with the electrolyte. Following Kjelstrup and Bedeaux (22) we obtain:

$$\sigma^s = J_q'^{i,o}\Delta_{i,s}\frac{1}{T} + J_q'^{o,i}\Delta_{s,o}\frac{1}{T} - \frac{j}{T^s}\left(\Delta_{i,o}\phi + \frac{1}{F}\Delta_n G^s\right) \quad [28]$$

Here i,o stands for a,e or e,c, while s refers to the electrode surface. The reaction Gibbs energy is computed for changes in neutral components in this description of the entropy production, where we emphasize the contributions to the measured electric potential difference. We have then from Eq.(1)

$$\Delta_n G^s = -\mu^s_{\mathrm{Li}}(T^s) \quad [29]$$

At reversible conditions $\sigma^s = 0$ and $T^i = T^s = T^o$. There are isothermal conditions in each electrode so $\Delta_{i,o}\phi + \frac{1}{F}\Delta_n G^s = 0$. The electric potential drop (the Nernst potential drop) at the electrode surface is thus

$$\Delta_{i,o}\phi = \frac{1}{F}\mu^s_{\mathrm{Li}}(T^s) \quad [30]$$

The same analysis applies for the cathode surface, with the reverse reaction of Eq.(1). When the electrodes on the two sides have the same composition, we obtain the total contribution from the electrode surfaces to the cell potential:

$$\Delta_{a,e}\phi + \Delta_{e,c}\phi = \frac{1}{F}\left[\mu_{\mathrm{Li}^{\mathrm{s,a}}}(T^{s,a}) - \mu_{\mathrm{Li}^{\mathrm{s,c}}}(T^{s,c})\right] = \frac{1}{F}S_{\mathrm{Li}}\Delta T \quad [31]$$

In the last equality, we used $\left(\partial\mu_j/\partial T\right)_x = -S_j$. We will evaluate S_j for the average temperature of the conductors, as we do not take second order effects into account. The entropy of Li is a function of its composition in CoO_2, and is measured by x, as in Li_xCoO_2.

$$S_{\mathrm{Li}} = S^0_{\mathrm{Li}} + R\ln x \quad [32]$$

In the present case, $x = 1$, and the entropy is the entropy of Li in the two-dimensional layer. This quantity is not known. The standard entropy of Li in the solid crystal state at 298 K is 29 J/K mol^{-1}.

The Seebeck coefficient at zero and infinite times

To summarize the derivations above, we have obtained the Seebeck coefficient for the initial homogeneous solutions as

$$\varepsilon_0 = \left(\frac{\Delta\phi}{\Delta T}\right)_{j=0,d\mu_{1,T}=0} = \frac{1}{F}\left(S_{\mathrm{Li}} + S^*_{\mathrm{e}^-} - S^*_{\mathrm{Li}^+} - \frac{t_1 q_1^* + t_2 q_2^*}{T}\right) \quad [33]$$

In full Soret equilibrium, when both diffusion processes have come to an end, we have

$$\varepsilon_{\infty,2} = \left(\frac{\Delta\phi}{\Delta T}\right)_{j=0,J_1=0} = \frac{1}{F}\left(S_{\mathrm{Li}} + S^*_{\mathrm{e}^-} - S^*_{\mathrm{Li}^+}\right) \quad [34]$$

When only one of the Soret-equilibria have been attained, we have

$$\varepsilon_{\infty,1} = \left(\frac{\Delta\phi}{\Delta T}\right)_{j=0,d\mu_{1,T}=0} = \frac{1}{F}\left(S_{\mathrm{Li}} + S^*_{\mathrm{e}^-} - S^*_{\mathrm{Li}^+} - \frac{t_1 q_1^*}{T}\right) \quad [35]$$

At an arbitrary time t, we use the symbol ε_t for the ratio $\Delta\phi(t)/\Delta T$.

Experimental

Materials

The electrolyte was a 1.0 M lithium hexafluorophosphate ($LiPF_6$)- solution. The solvent was a liquid mixture with weight ratio 50/50 of ethylene carbonate (EC) and diethyl carbonate (DEC). The solution was LP40 from BASF. Concentrations were given with an accuracy of 5%. Cells were made using the same batch. The ratio 50/50 gives a mole fraction of DEC equal to 0.43 with molar weights of EC and DEC equal to 88.06 and 118.13 g/mol, respectively.

A Whatman microporous glassfiber filter, no 1823070, was soaked with electrolyte before the electrodes were mounted. The electrode material, $LiCoO_2$, was Hohsen type electrode HS-LIB-P-Co-001. Electronic leads (current collectors) were made from aluminum foil. The electrode-electrolyte assembly was contained in a pouch cell sandwiched between two copper plates. The pouch material was a laminate of the polyester polyethlyene terephtalate (PET, 12 μm)/ aluminum (Al 9 μm) and polyethylene (PE 100 μm). The cell assembly was done in a glove box, with water < 1 ppm and oxygen < 5 ppm. The glass filter acted as a separator of the electrodes. After assembling the cell, the separator was dripped with electrolyte to ensure filter saturation.

The cell was sandwiched between copper plates that were thermostatted to $\pm 0.1^{\circ}$C by circulating water from a water reservoir. The thickness and thermal conductivity of all the layered materials are given in Table 1.

TABLE I. Thickness and thermal conductivity of cell materials.
*Reported only here. Measured as described in (24)

Part of the cell	**Thickness** $/10^{-3}$**m**	**Thermal conductivity** $/ W\ K^{-1}\ m^{-1}$	**Resistance** $/ 10^{3}\ W^{-1}\ K\ m^{2}$
Al connecting lead	0.014	237 (25)	$6 \cdot 10^{-5}$
Cu end plates	2.000	401 (25)	$5 \cdot 10^{-3}$
*Pouch cell laminate	0.132	0.25	0.53
$LiCoO_2$ electrode (LCO)	0.030	1.07 (24)	0.03
Electrolyte-soaked separator	1.787	0.19 (24)	9.40

Apparatus

The cell assembly is shown in Figure 2. The symmetric pouch cell was placed between two copper plates in contact with two aluminum plates. The temperature of each copper plate was controlled by the temperature of an external water reservoir (thermostat Grant GD 120). The copper plates and half cells were shielded from the outside and from each other by polyether ether ketone (PEEK). The temperatures inside the apparatus were measured using K-type precision fine wire thermocouples from Omega (see Figure 2). The average temperature in the cell was kept constant at (25.0 $\pm$0.1) $^{\circ}$C. The potential measurement started with the same temperature on each side to determine the bias potential of the cell. After that, the temperature in the external water reservoir was raised, while the other was

lowered, to set a gradient, keeping the same mean temperature. The potential and temperatures were measured continuously using the Agilent 3497A data acquisition unit. Time variations were recorded on a minute, hour and daily basis, to help reveal various transient phenomena.

In a good measurement, the cell should have at start a bias potential within a few mV. The bias potential was therefore measured before and after the experiment at isothermal conditions. The result was subtracted from the measured potential. Cell A had a bias potential near 0 mV, Cell B had a bias potential of -9.9 mV, and Cell C of 9.5 mV. Unless otherwise stated, the discussion and results are based on Cell A, while the results for the other cells can be used to give qualitative support to conclusions drawn for Cell A.

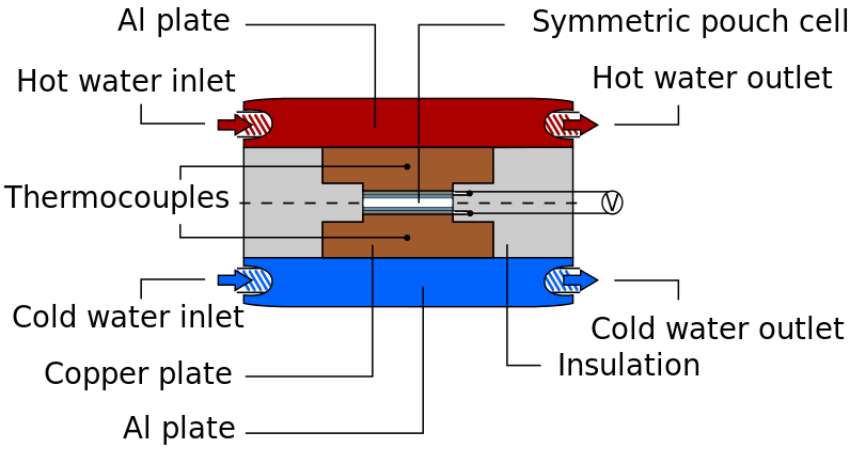

Figure 2. Sketch of the symmetric cell sandwiched between two copper plates. The temperatures of the copper are controlled by water flowing through aluminum plates from external water reservoirs. The copper plates and half cells were insulated from the surroundings and from each other. The potential difference was measured as a function of the temperature difference between the copper plates.

The cell temperature profile

The electrolyte sample contained in the microporous glass separator was chosen to be rather thick ($\approx$ 2 mm). The thermal resistances of the materials, listed in Table 1, show that the only other thermal resistance, relevant to the temperature profile across the cell, is that of the housing material. The other layers, including the electrode layers of $LiCoO_2$, are in good approximation isothermal.

The pouch cell was equipped with thermocouples positioned close to the electrodes inside the cell, see Fig.1. A temperature difference was established across the cell. The characteristic time needed to establish this profile across the sample can be estimated from the thermal diffusivity, $k/\rho C_p$. With a heat capacity, C_p, around 20 J/K mol, a thermal conductivity of k = 0.2 W/K m and a density ρ around 1 kg/m^3, the thermal diffusivity is such that the temperature gradient is established much before the temperatures of the external water baths have reached steady state (approximately 10 minutes).

At stationary state, the heat flux through the cell is constant, and the thermal resistances are additive. The ratio of the heat flux to the temperature difference

$$(J'_q)_{J_1=J_2=0} = \frac{\Delta_{\mathrm{tot}}T}{R_{\mathrm{tot}}} = \frac{\Delta T}{R} \qquad [36]$$

where tot means the whole series of the resistances taken in the stationary state. Absence of subscript refers to the resistance between the electrodes. The total thermal resistance can be estimated from values of the homogeneous layers:

$$R_{\mathrm{tot}} = 2\frac{x_{\mathrm{Cu}}}{k_{\mathrm{Cu}}} + 2\frac{x_{\mathrm{CH}}}{k_{\mathrm{CH}}} + 2\frac{x_{\mathrm{Al}}}{k_{\mathrm{Al}}} + 2\frac{x_{\mathrm{LCO}}}{k_{\mathrm{LCO}}} + \frac{x_{\mathrm{separator}}}{k_{\mathrm{separator}}} \qquad [37]$$

We are interested in the temperature difference across the $LiCoO_2$ and electrolyte parts, R. Equation (36) gives

$$\frac{\Delta T}{\Delta_{\mathrm{tot}}T} = \frac{R}{R_{\mathrm{tot}}} \qquad [38]$$

where R contains contributions from the electrolyte in the separator and the housing material (see equation above).

The ratio between the temperature across the electrodes, ΔT, and the externally applied difference, $\Delta_{\mathrm{tot}}T$, was determined in a special set-up for a series of 5 temperature differences between 5 K and 25 K. The special set-up was extra equipped with thermocouples next to the electrodes. The result was $\Delta T/\Delta_{\mathrm{tot}}T = 0.70 \pm 0.01$, independent of the value of the external temperature difference, in the range 5 K to 25 K. This uncertainty reflects the reproducibility of the experiments. With the available layers' thermal conductivity, we were also able to estimate the ratio. From the conductivities k_{i} and material thicknesses x_{i} listed in Table 1, we computed a ratio of 0.89. It is not unreasonable to compute a larger ratio than the experimental one, given that we did not include the unknown housing contact resistances in the calculation. Thermal losses along the current collectors are also neglected in the expression for R_{tot}. Another error source is the positioning of the thermocouples. They may be closer to each other inside the cell than the electrode surfaces are. We shall proceed with the experimental result, using an uncertainty of 10-15

Results

Time-evolution of the thermoelectric signal

The development of the thermoelectric potential of the cell, called simply the *emf* from now on, with time is given for three Cells, A, B and C, in Figure 3. The average temperature of all cells was 298 K and the temperature difference between the electrodes in all cells was 5.67 K. The temperature difference across the electrodes was computed from the calibration curve, as described above. The measurement started ($t = 0$) when the external water reservoirs had obtained the chosen temperatures. This happened after approximately 10 minutes, see the experimental section. All cells showed an initial peak after about 3 hrs, before a reduction in the signal took place. Some drift was observed in the base line signal

from Cells B and C, so the remaining experiments and results below are reported for Cell A.

It was possible to keep the stationary state shown in Cell A very much longer than shown in the figure, up to 4 *emf* $x10^4$ minutes (10 days). At some point the temperature difference was set back to zero. As a response a dip developed in the *emf* on the same time-scale as the peak appeared in the start of the experiment. Again, a slower process took over and reduced the signal back to the base line.

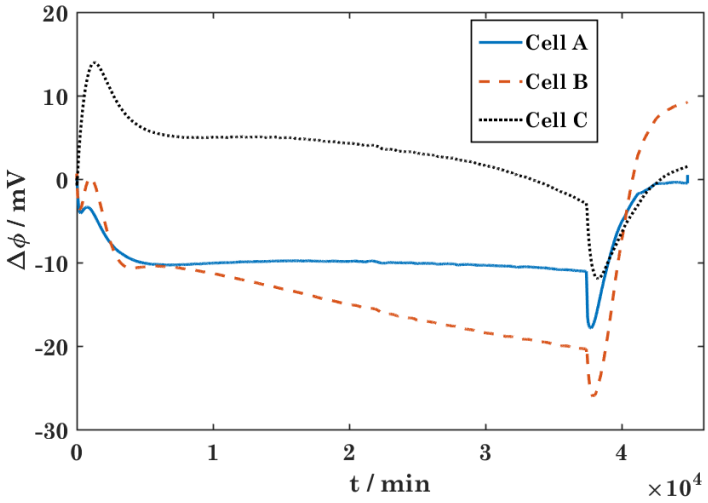

Figure 3. The electric potential variation with time in Cells A, B and C. The average temperature was 298 K and temperature difference between the electrodes was 5.67K.

Cell A was investigated for electrode temperature differences; 2.90 K, 5.67 K, and 7.84 K. The observed thermoelectric responses of the last two conditions are shown in Figures 4 and 5. The variations in the temperature difference, and the *emf* caused by this are plotted as a function of time. The temperature difference was stable within $\pm 0.1^{\circ}$C over time, see the horizontal (red) lines in the two figures.

The curves in Figures 4 and 5 have the same general trend as in Figure 3. In all figures, there is a peak reached within the first hours. The potential then decreases to a stationary value after around 5 hours. Setting the thermal driving force equal to zero in a next step, invariably leads to a relatively large dip in the signal, before its return to the baseline. A close-up of the curve in Fig.4 is shown in Fig. 6. The figure shows the time span relevant for battery charging and discharging.

The observations of a maximum in this figure around 750 minutes indicate that there are two dynamic phenomena competing with each other. Both phenomena are driven by the thermal force. We know that the thermal driving force will cause separation in the electrolyte (Soret effects), creating a chemical potential gradient that eventually balances the thermal force, cf. Eq.17. We assign the relatively fast first process, the initial increase in the potential, to component 1. The slower process, decreasing the potential to the final

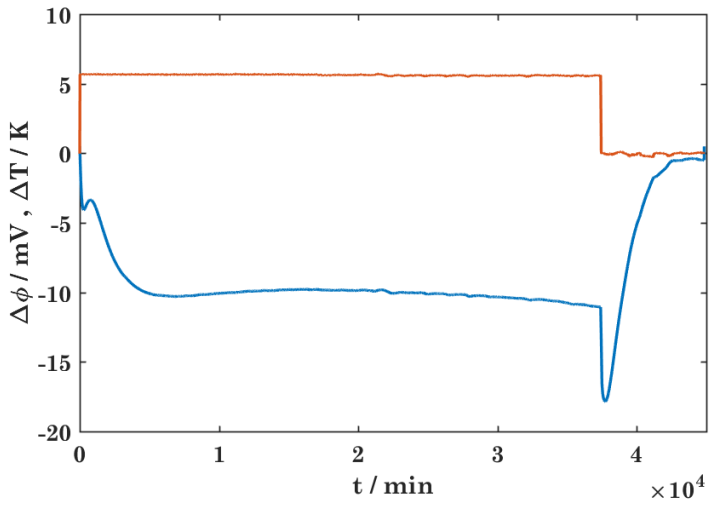

Figure 4. The time evolution of *emf* given a temperature difference of 5.67 K between the electrodes. The horizontal (red) line shows the temperature difference.

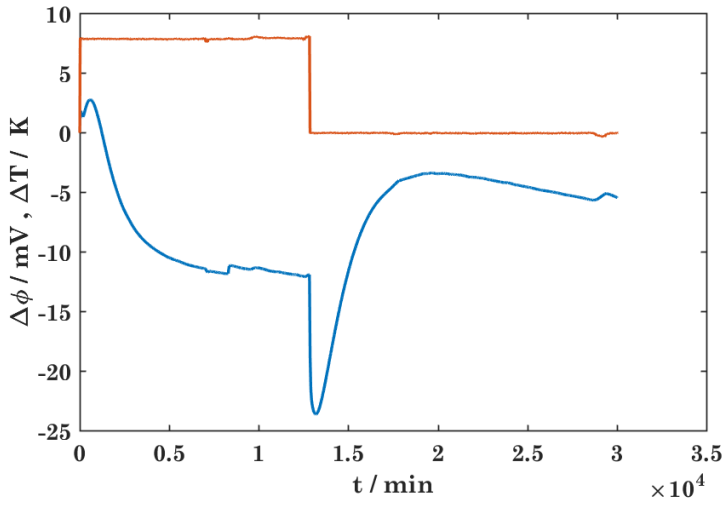

Figure 5. The time evolution of *emf* given a temperature difference of 7.84 K between the electrodes. The horizontal (red) line shows the temperature difference.

stationary state is due to component 2. A further assignment of the components, will be done once we have decomposed the data.

The interpretation is supported by the observations at the end of the experiment. When the temperature difference is set to zero, there exist gradients in chemical potential in the melt. A reduction in the gradient of component 1 explains the negative peak. The slower return to the base line is due to relaxation of the chemical potential gradient of component 2.

Single diffusion-type processes follow an exponential curve, as a concentration gradient builds or reduces exponentially with time (26). The temperature gradient was not established immediately, but took some 10 minutes to develop, and it is reasonable to assume

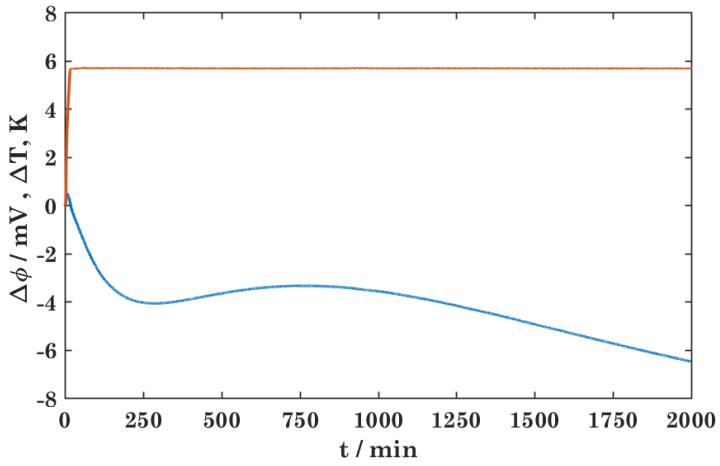

Figure 6. The time variation in Fig.4 on a smaller scale

that the onset of diffusion has already started before we measure the first thermoelectric potential peak.

The ratio of *emf* over the temperature difference at any time t, ε_t, is plotted in Fig. 7. We observe values ranging from 1.5 to -2.8 mV/K, varying over time. In the *absence* of diffusion, these three curves should collapse. This is not the case, because different chemical potential gradients have been created in the three cases. The lack of a common *initial* value for ε_t $(= \varepsilon_0)$ can only be understood if diffusion takes place. To use as the initial thermoelectric potential the value at $t = 0$ will underestimate ε_0. The true initial thermoelectric potential is thus not observed in the start of the experiment.

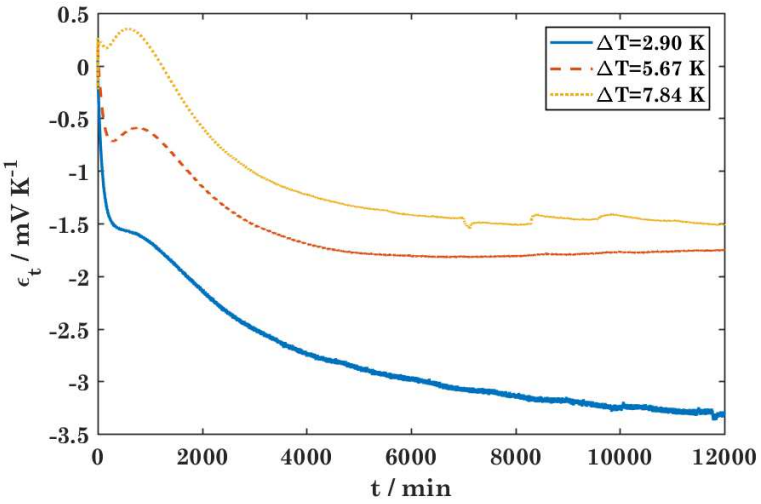

Figure 7. The *emf* divided by the temperature difference between the electrodes for Cell A.

The Seebeck coefficient at zero and infinite times. Peltier heats

The Seebeck coefficients at zero and infinite times can, nevertheless, be estimated from Figs. 4-5. The stationary flat parts in the figures give values for $\varepsilon_{\infty,2}$. The negative peak that occurs at the end of the experiment in Figs. 4-5, when ΔT is set to zero, is a measure of $\varepsilon_{\infty,1} - \varepsilon_0$. The difference between the depth of the negative peak and the bias potential, when the equilibrium state is reached, gives likewise an estimate for $\varepsilon_{\infty,2} - \varepsilon_{\infty,1}$. The values $\varepsilon_{\infty,1} - \varepsilon_0$ and $\varepsilon_{\infty,2} - \varepsilon_{\infty,1}$, were obtained from the curves in this way, and used to compute $\varepsilon_{\infty,1}$ and ε_0.

The results are shown in Table 2. The difference between the values in the two rows reflect the uncertainty in the experiment. The average results (bottom line) are therefore given with one significant cifer only.

The table shows that some of the Seebeck coefficients are rather large. For instance ε_0 is -2.8 mV/K, which is a very large value compared to values observed for semiconductors. Large values have been observed earlier with molten salts; ionic liquids (15, 17). The initial value can not be expected to hold when diffusion sets in. Interesting is the change in sign from the initial to the first stationary value. The negative value means that work can be obtained from the system. A positive value for the case that $J_1 = 0$ means that work must be used to maintain the salt separation that has been achieved across the electrolyte. The consequent separation of EC and DEC in the thermal field can, on the other hand, produce electric work, when the thermal force is removed.

TABLE II. Seebeck coefficients and electrode Peltier heats in homogeneous electrolytes and at Soret equilibrium (cf. text).

ΔT /K	ε_0 /mV K^{-1}	$\varepsilon_{\infty,1}$ /mV K^{-1}	$\varepsilon_{\infty,2}$ /mV K^{-1}	$S^*_{\mathrm{Li}^+}$ /J K^{-1} mol^{-1}
5.67	-2.5 ± 0.1	1.3 ± 0.1	-1.8 ± 0.1	214 ± 2
7.84	-3.1 ± 0.1	1.6 ± 0.1	-1.5 ± 0.1	181 ± 5
Average	-2.8 ±0.3	1.5 ±0.2	-1.7 ±0.2	197 ± 20
Peltier heats				
$LiCoO_2$ /kJ mol^{-1}	84 ±9	-45 ±6	51 ±6	
C /kJ mol^{-1}	-73 ±9	56 ±6	-40 ±6	

The Seebeck coefficients for the various conditions were used to compute the corresponding Peltier heats at an average operating temperature of 298 K. The Peltier heat $\pi = -TF\varepsilon$ represents in the present case, the heat change associated with the electrode reaction and the accompanying transport processes away from the electrode interface on both sides. We find a large and varying value in Table II. All values refer to one mole of electrons passing the outer circuit from the left to right electrode, and they reflect the changes on the cathode side. The value can even change sign, being large and positive at start (83 kJ/mol) and negative at intermediate times (-45 kJ/mol) before it reaches a final value (51 kJ/mol). It should be taken into account that the variation has a time schedule of days. One may speculate that the value observed by Huang *et al.* (12) can be compared to our intermediate value. In operation, when such an electrode in a Li-battery delivers charge, the changes are faster, and are accompanied by irreversible effects, Joule heat and

heat from the electrode overpotential. Knowledge of the separate contributions will enable us to model the temperature profiles when the battery is working. This is work for the future, however.

Knowing the reversible heat effect at the $LiCoO_2$-electrode, we may compute the corresponding value for the carbon electrode. We use the average value for the battery cycle taken from Viswanathan et al. (**?**), 36 J/K mol, and find that the electrode heat effects in a Li-battery at 298 K are surprisingly asymmetric, given the small entropy of the total reaction. The $LiCoO_2$ electrode heat varies from 51 to - 46 kJ/mol, while the carbon electrode will vary from -73 to 56 kJ/mol. This may explain why the reaction entropy depends largely on the state of charge. It may also be important for thermal modeling of the battery.

Thermal diffusion and heat of transfer

The time dependence of the thermoelectric potential can be used to model the cell. This was first done for cells with binary mixtures by de Groot (26), see also (11):

$$\varepsilon_t = \varepsilon_{\infty,i} - \frac{8(\varepsilon_\infty - \varepsilon_0)}{\pi^2} \exp(-\frac{t}{\theta_i}) \quad ,t > \theta/3 \qquad [39]$$

Where θ is the time constant given by:

$$\theta_i = \frac{h^2}{D_i \pi^2} \qquad [40]$$

Here h is the distance between the electrodes in the cell (1.787 mm) and D is the diffusion coefficient. The expression applies for values of t/θ_i larger than 0.3 (11, 26).

By inspecting the curves in Fig 4-5, we found above that two diffusion phenomena were present. The two processes are now assumed to be superimposed on one another. No model for ternary diffusion can be found in the literature. As a first approximation, we therefore used the transient model twice. We assume then that the composition gradient that arise after the first diffusion process has been completed, and becomes the starting point for the second diffusion process. To the analytical model above, we add a second exponential term. A third time-function $a(t)$ was also added to account for the equilibration of the apparatus after $t = 0$. The fit of this type of curve to the thermoelectric potential is shown for one case in figure 8. The fits resulted in the following expressions for ε_t (in mV/K) given the temperature differences 5.67 and 7.84 K:

$$\varepsilon_t = -a(t) - 49.6\exp(-0.003503 \cdot t) + 3.3\exp(-0.0007792 \cdot t) - 1.8$$
$$\varepsilon_t = -a(t) - 6.2\exp(-0.003679 \cdot t) + 3.4\exp(-0.0006462 \cdot t) - 1.5$$

The function captured the measured signal with a regression coefficient of 0.99. As initial Seebeck coefficient, we obtained 1.5 and 1.8 mV/K, in agreement with the average result in Table 2 (1.7 mV/K). The differences between the initial potential and the stationary state potential were next used to estimate the terms containing the heats of transfer, the

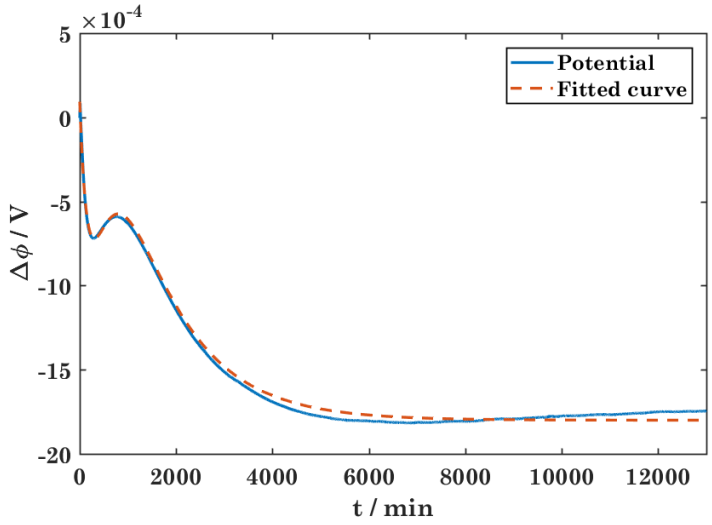

Figure 8. Fit of measured values for Cell A with temperature difference 7.84 K

characteristic times and the diffusion coefficients. The results are shown in Table 3.

The contributions to the electrode heats from the heats of transfer are significant for

TABLE III. Heats of transfer, characteristic times and diffusion coefficients of (1) and (2) in DEC. The errors are given in two standard deviations.

ΔT /K	$t_1 q_1^*$ /kJ mol^{-1}	$t_2 q_2^*$ /kJ mol^{-1}	θ_1 /min	θ_2 /min	D_1 /m^2 s^{-1}	D_2 m^2 s^{-1}
5.67	-34.4 $\pm$ 0.4	88.5 $\pm$ 0.3	285	1283	$1.89{\cdot}10^{-11}$	$4.20 \cdot 10^{-12}$
7.84	-43.0 $\pm$ 2.2	86.6 $\pm$ 1.2	272	1548	$1.98{\cdot}10^{-11}$	$3.48 \cdot 10^{-12}$
Average	-37 $\pm$ 7	87 $\pm$2				

both components. A value around -40 kJ/mol is typical for adsorption/desorption of polar molecules. The second process carries the signature of repulsion, 90 kJ/mol. Both transports have significant impacts on the electrode heat effect, on the time scale relevant to battery charging and discharging.

The two characteristic times were 280 and 1280 minutes (4.5 and 21.3 hours). The diffusion coefficients that correspond to this vary between 1 and 2 $\cdot 10^{-11}$ m^{2}s^{-1}. They are smaller by one order of magnitude than values observed for self diffusion in the literature, $2{\cdot}10^{-10}$ m^{2}s^{-1} (18). The diffusion of (1) is about twice as fast as the diffusion of the other component, see Table 3. This is exactly the ratio observed for self diffusion of EC over self diffusion of the ions (18). It is then tempting to relate the fast process to interdiffusion of EC-DEC, while the slower process is attributed to the interdiffusion of salt in DEC. More experiments are needed to confirm this interpretation. We can use the term $t_1 q*_1$ to estimate the Soret coefficient from Eq. 16. The ratio $t_1 q*_1 / RT^2$ becomes 0.06. The ratio of the thermal diffusion coefficient to the interdiffusion coefficient is then reasonable, a value near 0.1. We have not yet introduced a number for the transference coefficients. If the hypothesis is correct, that component 1 is the salt, we can use $t_{Li^+} = 0.4$ from Valøen and Reimers (23), giving $t_1 = t_{Li^+} - 1 = -0.6$. we see then that $q*_1$ becomes positive. More experiments are needed to establish this.

Conclusion

We have reported Sebeeck coefficients for the $LiCoO_2$-electrode and Li-battery relevant electrolyte $LiPF_6$ in ethylene and diethyl carbonate at initial and infinite times, ranging from -2.8 to 1.5 mV/K. These values mean that the reversible electrode heat is large, varying from 84 to -45 kJ/mol at 298 K. The electrolyte of Li-batteries has often been considered as uniform in the literature. This work has shown that relatively large concentration gradients can arise in a thermal field. In the modeling of thermal effects the Soret and Seebeck effects that follow are clearly significant.

Acknowledgment

The group of authors acknowledge the Research Council of Norway (RCN) project no. 228739, for funding through the project "Life and Safety for Li-ion batteries in Maritime conditions (SafeLiLife)". Henrik Eriksson at Uppsala University is thanked for help to make the pouch cells. We acknowledge ENERSENSE for financial support. SK is also grateful to RCN through its Centers of Excellence funding scheme, project number 262644, PoreLab.

References

1. U. S. Kim, J. Yi, C. B. Shin, T. Han, and S. Park. *J. Power Sources*, 196(11):5115 – 5121, 2011.
2. L. Cai and R. E. White. *J. Power Sources*, 196(14):5985 – 5989, 2011.
3. Y. Ye, Y. Shi, N. Cai, J. Lee, and X. He. *J. Power Sources*, 199:227 – 238, 2012.
4. W. Walker and H. Ardebili. *J. Power Sources*, 269:486 – 497, 2014.
5. N. Damay, C. Forgez, M.-P. Bichat, and G. Friedrich. *J. Power Sources*, 283:37 – 45, 2015.
6. S. Al Hallaj, H. Maleki, J.S. Hong, and J.R. Selman. *J. Power Sources*, 83(1-2):1 – 8, 1999.
7. C. Alaoui. *IEEE Trans. Veh. Technol.*, 62(1):98–107, 2013.
8. X. Hu, S. Asgari, S. Lin, S. Stanton, and W. Lian. A linear parameter-varying model for hev/ev battery thermal modeling. In *2012 IEEE Energy Conversion Congress and Exposition (ECCE)*, pages 1643–1649, 2012.
9. V. V. Viswanathan, D. Choi, D. Wang, W. Xu, S. Towne, R. E. Williford, J.-G. Zhang, J. Liu, and Z. Yang. *J. Power Sources*, 195(11):3720 – 3729, 2010.
10. O.S. Burheim, M.A. Onsrudc, J.G. Pharoahd, F. Vullum-Bruer, and P.J.S. Vie. *ECS Transactions*, 58:145 – 171, 2014.
11. H.J.V. Tyrrell. *Diffusion and heat flow in liquids*. Butterworths, London, 1961.
12. Q. Huang, M. Yan, and Z. Jiang. *J. Power Sources*, 156(2):541 – 546, 2006.
13. O. Burheim and P.J.S. Vie and S. Møller-Holst and J. Pharoah and S. Kjelstrup. *Electrochim. Acta*, 55:935–942, 2010.
14. B. Flem and S. Kjelstrup and Å. Sterten. *Light Metals*, pages 203–209, 1996.
15. B. Flem and Q. Xu and S. Kjelstrup and Å. Sterten. *J. Non-Equilib. Thermodyn.*, 26: 125–151, 2001.

16. T. Motohashi, Y. Sugimoto, Y. Masubuchi, T. Sasagawa, W. Koshibae, T. Tohyama, H. Yamauchi, and S. Kikkawa. *Phys. Rev. B*, 83:195128, May 2011.
17. Q. Xu, S. Kjelstrup and B. Hafskjold. *Electrochim. Acta*, pages 2597–2603, 1998.
18. K. Hayamizu. *J. Chem. Eng. Data*, 57:2012–2017, 2012.
19. L.E. Bell. *Science*, 321:1457–1461, 2008.
20. S. Jeong, M. Inaba, Y. Iriyama, T. Abe, and Z. Ogumi. *Electrochim. Acta*, 47:1975–1982, 2002.
21. S. Kjelstrup and D. Bedeaux. *Non-equilibrium thermodnamics of heterogeneous systems*. World Scientific, 2008.
22. S. Kjelstrup and D. Bedeaux. *Thermodynamics of Electrochemical Systems Chapter 4, in Springer Handbook of Electrochemistry, Part A*, pages 69–93. Springer, 2016.
23. L.O. Valøen and J.N. Reimers. *J. Electrochem. Soc.*, 152:A882–A891, 2005.
24. F. Richter, P. J.S. Vie, S. Kjelstrup, and O. S. Burheim. *Electrochimica Acta*, 250 (Supplement C):228 – 237, 2017.
25. G.H. Aylward and T.J.V. Findlay. *SI Chemical Data, 6th edition*, volume 6. Wiley, 2008.
26. S.R. de Groot. *Physica*, IX:699–708, 1942.